catalysts

MDPI

Review

Recent Progress of Metal-Oxide-Based Catalysts for Non-Oxidative Coupling of Methane to Ethane and Hydrogen

Junbu Wang [1,2,†], Zhiqiang Rao [1,2,†], Zeai Huang [1,2,*], Yaolin Chen [1,2], Fang Wang [2] and Ying Zhou [1,2,*]

[1] State Key Laboratory of Oil and Gas Reservoir Geology and Exploitation, Southwest Petroleum University, Chengdu 610500, China
[2] School of New Energy and Materials, Southwest Petroleum University, Chengdu 610500, China
* Correspondence: zeai.huang@swpu.edu.cn (Z.H.); yzhou@swpu.edu.cn (Y.Z.)
† These authors contributed equally to this work.

Abstract: Methane is the fundamental raw material of the C1 chemical industry, with abundant reserves. Its direct conversion into high-value-added chemicals has great scientific significance and broad commercial potential for the efficient use of methane resources. However, it is difficult to convert methane into more useful hydrocarbons and hydrogen, as the reaction usually requires external energy to overcome thermodynamic limitations. Non-oxidative coupling of methane to produce ethane and hydrogen is a promising supply technology. Catalysts which can be adapted to various energy sources are key to this technology. In recent years, considerable progress has been made in the design and application of these thermal and photocatalysts. This review outlines some typical catalysts, and reviews the progress in the understanding of reaction mechanisms. Finally, suggestions for the development of high-selectivity and high-stability catalysts for the future are presented.

Keywords: photocatalysis; thermal catalysis; non-oxidative coupling of methane; ethane; hydrogen

check for updates

Citation: Wang, J.; Rao, Z.; Huang, Z.; Chen, Y.; Wang, F.; Zhou, Y. Recent Progress of Metal-Oxide-Based Catalysts for Non-Oxidative Coupling of Methane to Ethane and Hydrogen. *Catalysts* **2023**, *13*, 719. https://doi.org/10.3390/catal13040719

Academic Editor: Carl Redshaw

Received: 14 March 2023
Revised: 29 March 2023
Accepted: 30 March 2023
Published: 10 April 2023

Copyright: © 2023 by the authors. Licensee MDPI, Basel, Switzerland. This article is an open access article distributed under the terms and conditions of the Creative Commons Attribution (CC BY) license (https://creativecommons.org/licenses/by/4.0/).

1. Introduction

With the global temperature rising each year, climate anomalies are becoming more and more frequent, greatly impacting the bulk commodity market, especially in energy. Consequently, the utilization of clean energy natural gas is rapidly expanding with the exploitation of shale gas and combustible ice [1]. In the past, natural gas was mainly used as fuel [2], but now, in order to achieve green and sustainable development of the energy system, its industrial utilization is gaining more attention [3].

Natural gas is mainly composed of methane (CH_4)-the basic raw gas of the C1 chemical industry. Thus, the conversion of CH_4 to high-value chemicals (such as hydrogen (H_2), alcohols, alkanes, and olefins) is a promising technology in chemical and energy supply. Traditionally, these chemicals are obtained through the indirect conversion of CH_4, that is, CH_4 is first converted into syngas (CO and H_2), and then processed through the Fischer–Tropsch process. Unfortunately, this method has some disadvantages, such as a complicated process, low utilization rate of CH_4, high energy consumption, and high cost [4,5].

The industry has been seeking cost-effective and low-carbon ways to utilize CH_4, of which ethene (C_2H_6) is a highly important commodity chemical for many manufacturing products [6]. Non-oxidative coupling of methane (NOCM) produces C_2H_6 and H_2 (Equation (1)), making it the simplest C-C coupling process and a model reaction for converting CH_4 to multi-carbons.

$$2CH_4 \rightarrow C_2H_6 + H_2 \ \Delta H\ (298K) = 68.6\ kJ\ mol^{-1} \quad (1)$$

However, the thermodynamic barrier of this reaction necessitates the use of energy sources to trigger CH_4 coupling [2,7], such as thermal catalysis and photocatalysis. Thermal

catalysis is the most common method, but carbon deposition occurs easily at relatively high temperatures (>773 K) [8] and complete dehydrogenation of CH_4 reduces C_2H_6 selectivity. Solar energy, on the other hand, is the richest and cleanest renewable energy and has been used to promote NOCM reactions under mild conditions [9,10], improving system safety and reducing reaction temperature.

From an economic standpoint, Gerceker et al. suggested that the selectivity of C_2H_6 should be at least 25% and coke formation should be less than 20%, making it a viable option for commercial applications [11]. Additionally, CH_4 conversion efficiency should be taken into consideration. To this end, this paper reviews a series of catalysts from the perspective of catalytic efficiency and the mechanism of typical thermal catalysis and photocatalysis in NOCM reactions. In thermal catalysis, the catalysts reduce the reaction barrier and regulate the reaction intermediates in the "adsorption-activation-desorption" process. For photocatalysis, catalysts with different electronic properties are excited by solar energy to regulate the C-C coupling process. An overview of the properties and mechanism of the active catalysts is provided, as well as factors that affect CH_4 activation and C_2H_6 selectivity. Designing efficient catalysts for direct NOCM is of great importance for the future.

2. Thermal Catalytic NOCM

2.1. Fundamentals of Thermal Catalysis

Generally, it is assumed that the reaction of Thermal Catalytic NOCM consists mainly of three processes [12]: (1) CH_4 is adsorbed onto the active site of the catalyst; (2) the C-H bond is dissociated by the active component and forms adsorbed methyl or H_2; (3) the identical adsorbed groups are coupled, then desorbed to generate C_2H_6 and H_2 in the gas phase. However, as the most stable alkane, the CH_4 molecule is sp^3 hybrid [13] and its C-H bond dissociation energy is up to 439 kJ mol^{-1} [14,15], making the activation energy of the reaction extremely high, despite the catalyst reducing the energy effectively. The first C-H bond breaking of CH_4 is more difficult, whereas the successive dehydrogenation reaction is easy to occur, thus leading to methyl cracking without needing a coupling process.

In thermal catalytic NOCM, the C-H bond of the CH_4 molecule is broken through high-temperature thermal energy. The generation of reaction intermediates is regulated by introducing a thermal catalyst, thus avoiding the fracture of the CH_3-CH_3 skeleton, and effectively improving the catalytic performance. Some typical thermal catalysts are summarized in Table 1.

Table 1. C_2H_6 selectivity and CH_4 conversion in thermal catalytic NOCM using different catalysts.

Entry	Catalysts	Temperature (K)	Reaction Conditions	C_2H_6 Selectivity (%)	CH_4 Conversion (%)	Reference
1	Pt	523	100 mg, 400 mL min^{-1} CH_4	-	19.3	[16]
2	Pt/CeO_2	1053	0.36 g, 0.094 h^{-1} CH_4	84.8	7.92	[17]
3	Pd/α-Al_2O_3	550	300 mg, 300 mL min^{-1} CH_4	4	-	[18]
4	Pt/Mo_2TiC_2	1023	50 mg, 12.9 GHSV(h^{-1})	85	6.5	[19]
5	Fe©SiO_2	1223	4.84 L g_{cat}^{-1} h^{-1} CH_4	2	15	[20]
6	Pt1@CeO_2	1173	0.2 g, 20 mL min^{-1} CH_4	43.6	~6	[21]
5	Fe/SiO_2	1293	1.2 g, 2.4 mL g_{cat}^{-1} s^{-1}	13	12.2	[22]
6	Fe/HZSM-5	973	0.5 g, 6L g_{cat}^{-1} h^{-1} CH_4	23	3	[12]
7	Fe©SiO_2	1098	100 mg, 20 mL min^{-1} CH_4	80	15	[23]
8	Fe©SiO_2	1353	0.6 g, 8000 mL g_{cat}^{-1} h^{-1} CH_4	7.9	6	[24]
9	Ta/SiO_2	573	300 mg, 30 mL min^{-1} CH_4	50	0.1	[25]
10	$NiOx/SiO_2$	700	300 mg, 300 mL min^{-1} CH_4	16	-	[26]

2.2. Precious Metal Catalysts

Noble metal catalysts can more effectively control the adsorption and desorption of intermediate products in thermal catalytic NOCM, thus enabling the directional conversion of CH_4 to C_2H_6 [19]. In 1991, Belgued et al. [17] explored the effect of temperature on the selectivity of C_2H_6 over Pt/CeO_2 catalyst (Figure 1a,b). With increasing temperature, the adsorption of methyl (-CH_3) on the Pt surface decreased, whereas the formation of

intermediates such as -CH_2, -C_2H_3, and -C_2H_2 accelerated, thus reducing the selectivity of C_2H_6. Moya et al. [18] confirmed that the highly dispersed Pd active sites chemisorbed intermediate carbon species, promoting the desorption balance of methyl (-CH_3) and proton hydrogen (H) over a Pd/α-Al_2O_3 catalyst during the coupled hydrogenolysis of CH_4 at low temperature (500–750 K) (Figure 1c). Thermodynamic constraints in the thermal catalytic reaction motivate research into CH_4 activation at high temperatures. However, traditional metal cluster catalysts suffer from severe coking and significant deactivation in the high-temperature catalytic process. Xie et al. [21] used a single atom Pt_1@CeO_2 catalyst to achieve a 40 h catalytic cycle (1173 K). The continuous desorption of intermediates (-CH_3 and -CH_2) at atomically dispersed Pt sites improves the effective collision of carbon-containing intermediates on the surface of active sites and inhibits carbon deposition, which covers the active sites, thereby aiding the dynamic stability of the catalyst structure. In conclusion, it can be stated that precious metal catalysts can facilitate the adsorption energy of -CH_3 on the catalyst surface under appropriate catalytic temperature conditions, while inhibiting the adsorption of H atoms by unsaturated coordination carbon-containing intermediates, thus enhancing the effective collision between adsorbed CH_3, and consequently promoting the coupling stability of C_2H_6. Recently, Pt nanolayers anchored at the hexagonal close-packed sites of the MXene support were able to activate the primary C-H bond of CH_4 to create methyl radicals that favor desorption over subsequent dehydrogenation, suppressing coke deposition. At 973 K, the catalyst could operate continuously for 72 h without deactivation and CH_4 conversion reached 7% (Figure 1d,e) [19].

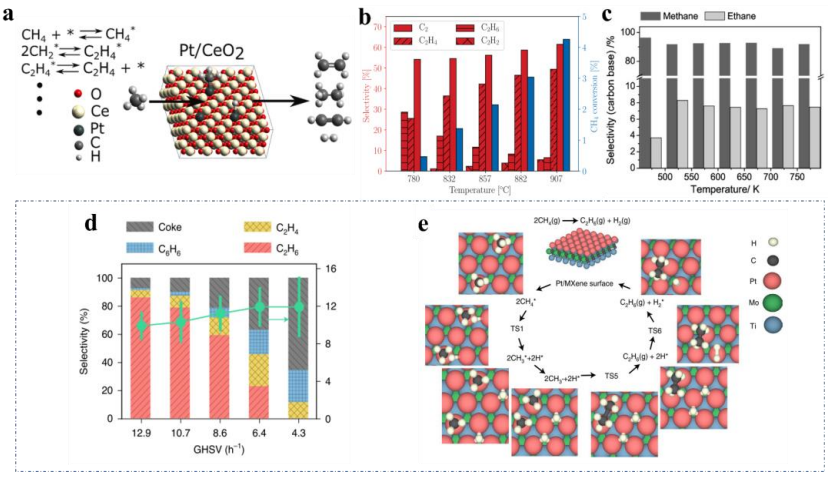


Figure 1. (**a**) Reaction mechanism of Pt/CeO_2 catalyst [17], (**b**) CH_4 conversion and C_2 selectivity on Pt/CeO_2 catalyst [17], copyright 2020, Elsevier. (**c**) Conversion of CH_4 and C-based selectivity to C2 products [18], copyright 2011, Elsevier. (**d**) Catalytic performance of Pt/$Mo_2TiC_2T_x$ for non-oxidative coupling of CH_4, and (**e**) a proposed catalytic circle of NOCM over Pt/$Mo_2TiC_2T_x$ catalyst [19]. Copyright 2021, Springer Nature.

2.3. Non-Precious Metal Catalysts

Compared with expensive precious metals, relatively cheaper non-precious metal catalysts such as Fe have been found to successfully catalyze the direct dehydrogenation of CH_4 to generate carbonaceous metal compounds (MeC_x) [13,27], resulting in improved stability of the catalyst even under high-temperature conditions. In 2014, Bao et al. [20] used an Fe©SiO_2 catalyst to achieve catalytic stability for 60 h continuously, with a selectivity of C_2H_6 of around 3% at 1223 K (Figure 2a,b). FeO_x is confined in the SiO_2 lattice, with -CH_3 species released from the constrained Fe atom. After CH_4 is completely dehydrogenated, the carbon species are directly converted into a FeC_x solid solution from the C-Fe=CH_2 structure, avoiding carbon deposition. Kim et al. [22] found that the concentration of -CH_3 species affects the catalytic process, with a high concentration of -CH_3 ($\log_{PCH3} > -2$) atmosphere being conducive to the formation of C_2H_6. Conversely, low concentrations of -

CH_3 ($log_{PCH3} < -3$) conditions result in C_2H_6 continuing to dehydrogenate as a medium for the formation of C_2H_4 or C_2H_2 (Figure 2c). It was shown that by regulating the formation energy of -CH_3 species over Fe©CRS (CRS:SiO_2) catalyst at 1353 K, catalytic stability could be achieved for 50 h, with a selectivity of C_2H_6 maintained at 7.9%. Mechanism studies confirmed that the energy barrier to be overcome for complete CH_4 cracking on the confined Fe_3C surface (ΔG = 1.1 eV) is lower than that of the pure Fe_3C surface (ΔG = 2.8 eV) (Figure 2d), with the formation energy of -CH_3 species on the restricted Fe_3C surface site being lower than that of the pure Fe_3C site (Figure 2d). Li et al. [28] proposed a quasi "Mars-van Krevelen" surface reaction mechanism, and research showed that the extraction and refilling of surface carbon atoms was the key to the transformation of surface carbon species. The -CH_3 species on the surface of Fe_1©SiO_2 catalyst are difficult to desorb into the gas phase at the single iron atom site, whereas the carbon sites adjacent to the iron atom are more likely to desorb -CH_3 and transfer protons H, thereby promoting the cyclic conversion of carbon atoms on the surface. Kashaboina et al. [29] confirmed that the in situ transformation of the unsaturated coordination structure of the In-C bond is a necessary condition for the formation of C_2H_6 on In/SiO_2 catalyst by in situ X-ray absorption spectroscopy. Moya and Rashid et al. [26,30] proved that Ni^{2+} is conducive to CH_4 adsorption, with the CH_4 adsorption capacity of the catalyst containing Ni^{2+} being 13 times that of the catalyst containing Ni^0. Dipu et al. [23] found that the selectivity of C_2H_6 can reach 80% on the variable valence metal Ni-P/SiO_2 catalyst at 1098 K (Figure 2e). Lin et al. [31] showed that the divalent metal Ta^{2+} site is the active center on the Ta/SiO_2 catalyst, with the Si-O-Ta bond in $(-SiO_3)_2Ta$ being broken and the H_2-Ta-CH_2CH_3 structure formed during activation of CH_4, which can then be dehydrogenated to Ta-H and C_2H_6. Soulivong et al. [25] achieved a selectivity of the products of around 50%, with catalytic stability maintained for 200 h over Ta/SiO_2 catalyst at 573 K. Therefore, non-precious metal catalysts can promote the C-C coupling of CH_4 through a "restriction strategy" or "metal valency change strategy" to obtain the target products of C_2H_6 and H_2.

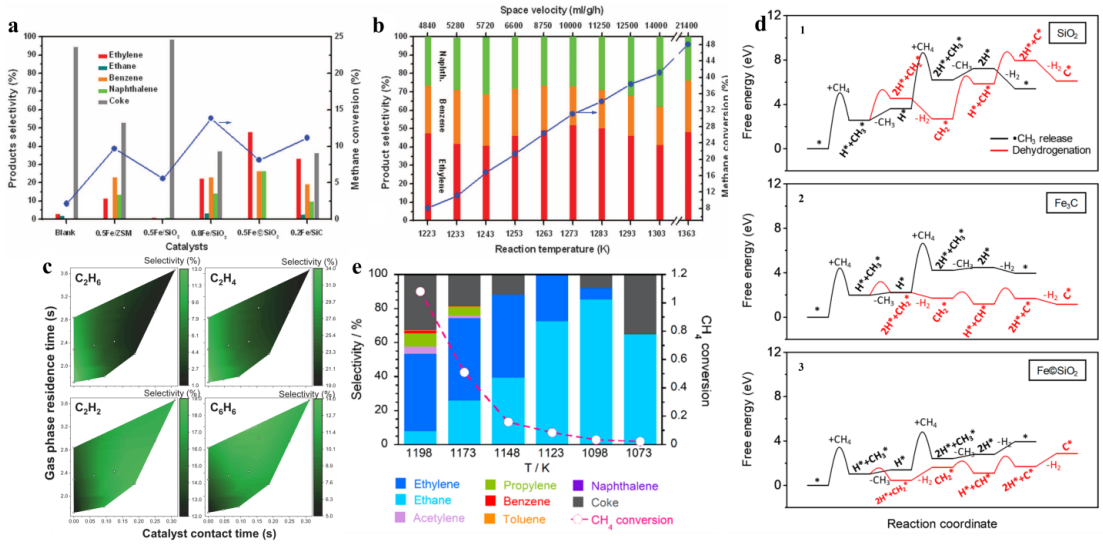


Figure 2. (**a**) Comparison of different catalysts at 1223 K [20], (**b**) effect of reaction temperatures and space velocities on the 0.5% Fe©SiO_2 catalyst. Blue circles denote CH_4 conversion, whereas bars represent product selectivity, CH_4 conversion, and C_2 hydrocarbon selectivity over Fe©SiO_2 catalyst [20], copyright 2014, The American Association for the Advancement of Science. (**c**) C_2H_6, C_2H_4, C_2H_2, and C_6H_6 selectivity as functions of catalyst contact time and gas-phase residence time. Experimental NOCM results using Fe@CRS catalyst in a fixed-bed reactor [22], copyright 2020, Springer Nature. (**d**) The activation energy barrier of CH_4 on SiO_2, Fe_3C, and Fe©SiO_2 catalysts [24], and (**e**) product distribution and CH_4 conversion on Ni-P/SiO_2 catalyst as a function of temperature [23]. Copyright 2020, American Chemical Society.

3. Photocatalytic NOCM

3.1. Fundamentals of Photocatalysis

In the photocatalytic NOCM process involving a semiconductor catalyst, solar energy is utilized to stimulate the catalyst, creating photogenerated carriers (electrons and holes) [15]. The generated holes at the valence band trigger CH_4 to enter an excited state, forming methyl radicals ($\bullet CH_3$) and H protons ($CH_4 + h^+ \rightarrow \bullet CH_3 + H^+$). Subsequently, methyl radicals are combined to yield adsorbed C_2H_6 ($2\bullet CH_3 \rightarrow C_2H_6$), whereas the protons H are reduced by electrons to give adsorbed H_2 ($2H^+ + 2e^- \rightarrow H_2$) [32]. Finally, C_2H_6 and H_2 are desorbed in the CH_4 conversion process at low temperatures [33].

Moreover, several catalysts with no inherent semiconductor characteristics are also applied for photocatalytic NOCM, which are distinguished by dispersing highly active centers on non-photoresponsive insulator supports and localizing on specific sites by taking advantage of the interaction between active components and supports. Some typical photocatalysts that can improve CH_4 conversion or C_2H_6 selectivity are summarized in Table 2.

Table 2. C_2H_6 selectivity and CH_4 conversion in photocatalytic NOCM using different catalysts.

	Catalysts	Reaction Conditions	C_2H_6 Selectivity (% or μmol g^{-1} h^{-1})	CH_4 Conversion (% or μmol g^{-1} h^{-1})	Reference
1	SiO_2-Al_2O_3	250 W Xe lamp, 1.0 g, 100 μmol CH_4	0.01	5.9	[34]
2	FSM-16	300 W Xe lamp, 0.2 g, 200 μmol CH_4	1.63	5.7	[35]
3	ZrO_2/SiO_2	250 W Xe lamp, 0.5 g, 200 μmol CH_4	0.11	0.1	[36]
4	SiO_2-Al_2O_3-TiO_2	250 W Xe lamp, 1.0 g, 200 μmol CH_4	2.07	2.5	[37]
5	SiO_2-Al_2O_3-TiO_2	250 W Xe lamp, 1.0 g, 200 μmol CH_4	2.07	3.7	[38]
6	Nb-TiO_2-SiO_2	300 W Xe lamp, 0.1 g, 1 mL CH_4	1.7 μmol g^{-1} h^{-1}	3.5 μmol g^{-1} h^{-1}	[39]
7	Ag/MFI	250 W Xe lamp, 0.2 g, 200 μmol CH_4	4.40	4.0	[40]
8	Ga-ETS-10	high-pressure Hg lamp, 0.2 g, 200 μmol CH_4	70	15	[41]
9	Ag-HPW/TiO_2	400 W Xe lamp, 0.1 g, 0.3 MPa CH_4	150 μmol g^{-1} h^{-1}	4.96	[2]
10	Ce/SiO_2	300 W Xe lamp, 0.2 g, 200 μmol CH_4	94	13	[42]
11	Ce/Al_2O_3	300 W Xe lamp, 0.2 g, 200 μmol CH_4	20	15	[43]
12	Zn^{2+}-ZSM-5^-	high-pressure Hg lamp, 1.0 g, 200 μmol CH_4	99	6 μmol g^{-1} h^{-1}	[44]
13	Ga_2O_3	300 W Xe lamp, 0.2 g, 200 μmol CH_4	86	17	[45]
14	Pt/Ga_2O_3	300 W Xe lamp, 0.2 g, 1 mL CH_4	90	140 μmol g^{-1} h^{-1}	[46]
15	Pd/Ga_2O_3	300 W Xe lamp, 0.8 g, 30 mL min^{-1} CH_4	0.125 μmol g^{-1} h^{-1}	-	[32]
16	Pd-Bi/Ga_2O_3	300 W Xe lamp, 0.8 g, 450 h^{-1} CH_4	97	0.03	[47]
17	Pt/HGTS	300 W Xe lamp, 0.2 g, 44.6 μmol CH_4	3.48 μmol g^{-1} h^{-1}	28	[48]

3.2. Metal-Oxide-Based Catalysts

In 1998, Yoshida et al. [34] first reported that a SiO_2-Al_2O_3 catalyst could be utilized for NOCM, but its C_2H_6 selectivity was limited to 0.01%. Subsequently, Yoshida et al. found that high-energy ultraviolet light could induce the CH_4 molecule to transition directly from its ground state to an excited state, and the phosphorescent excitation sites of SiO_2 could desorb hydroxyl (-OH) groups from the surface [49]. Yuliati also confirmed that the dehydroxylation of SiO_2 could be achieved by two active sites, namely, the ≡Si–O• (NBOHC, non-bridging oxygen hole center) and the •Si≡ (E′ center, dioxasilirane group), with electrons being obtained at the NBOHC site and holes generated at the E′ center site [35].

To further increase the light absorption capacity of the catalyst, some researchers have introduced the highly dispersed photoactive component TiO_2. In 2002, Yoshida et al. [37,38] reported that a ternary oxide catalyst of SiO_2-Al_2O_3-TiO_2 achieved a C_2H_6 selectivity of 2.07%. The mechanism study showed that CH_4 was activated by ultraviolet light, and its surface hydroxyl groups desorbed to form $(SiO)_3$Ti-O-Al$(OSi)_3$, which acted as a highly active synergistic site to promote the electron transfer from the

oxygen center to the titanium site [38]. In 2021, Zhang et al. [39] proposed an efficient "coupling-desorption mechanism" strategy to regulate the yield of C_2H_6, with the yield of C_2H_6 reaching 1.7 μmol g^{-1} h^{-1} over the *n*-type semiconductor Nb-TS (single atom Nb-doped TiO_2-SiO_2) catalyst (Figure 3). Nb doping replaced the six coordinated Ti6c sites, generating additional active sites to provide additional local electrons which facilitated the directional migration of electrons to local •CH_3, thereby accelerating the coupling between CH_3-CH_3 species and desorbing more C_2H_6.

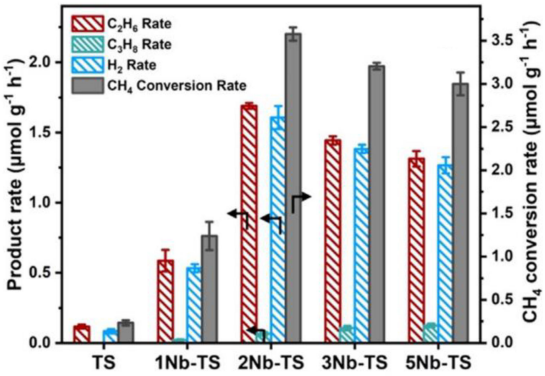


Figure 3. The hydrocarbon products, H_2 yields, and the CH_4 conversion rate over Nb-T [39]. Copyright 2021, John Wiley and Sons.

Based on the above research, it can be determined that in the photocatalytic NOCM process, metal oxide catalysts mainly utilize high-energy ultraviolet light to induce CH_4 to directly transition from the ground state to the excited state, and then adjust the surface electron transfer process through the oxide surface adsorption characteristics, thus improving CH_4 conversion and C_2H_6 selectivity by promoting the formation of adsorbed protons (H) and adsorbed •CH_3.

3.3. Metal-Modified Catalysts

The semiconductor catalyst has fixed intrinsic characteristics, making it difficult to meet the needs of photocatalytic reactions. Therefore, it is necessary to adjust the electronic structure of the catalyst by modifying the cocatalyst to optimize its catalytic performance. One strategy is to use metal-modified catalysts to broaden the light response region and improve the conversion efficiency of solar energy. Moreover, metal-modified photocatalysts can generate hot electrons or local electric fields to activate the C-H bond of CH_4, promoting the reaction [50]. The metal can also undergo a change from Me^{1+x} to Me^{x} during the reaction, which regulates the adsorption-desorption reaction involving CH_4 [50,51].

Yoshida et al. [42,43] found that adjusting the metal loading could achieve metal valence state modulation, thereby modifying the selectivity of C_2H_6. Ce^{3+} promotes fast electron migration in the low-loaded $Ce_{(0.01–0.1\%)}/SiO_2$ catalyst, resulting in C_2H_6 selectivity of up to 60%. However, a higher loading of Ce(2–5%)/SiO_2 catalyst yields a selectivity of 99% due to Ce^{4+} widening the band gap and inhibiting CH_3 dehydrogenation. Later, Yoshida et al. [40] proposed the "Ag^+-Ag^0-Ag^+ cycle balance charge" mechanism, and a C_2H_6 selectivity of 4.40% was achieved over Ag-MFI (MFI: SiO_2-$A1_2O_3$) catalyst. The photoexcited Ag^+ adsorbs CH_4 to form a complex (ZO-(Ag^+-CH_4)), which promotes the adsorption of CH_4. During the conversion of Ag^+ to Ag^0, the C-H bond is broken and •CH_3 species accumulate on the catalyst surface, increasing the C-C collision opportunity to form C_2H_6. In 2020, Yu et al. [2] confirmed the reversibility of "Ag^+-Ag^0-Ag^+" over the Ag-HPW/TiO_2 catalyst. The yield of C_2H_6 was found to reach 150 μmol g^{-1} h^{-1}, and the optical quantum efficiency was 3.5% (362 nm). It was further demonstrated that during the photocatalytic CH_4 coupling reaction, the Lewis acid sites around the low coordination Ag^+ are converted into Brønsted acid, and the Ag^0 formed in situ is the active center site for the generation of •CH_3 (Figure 4a,b).

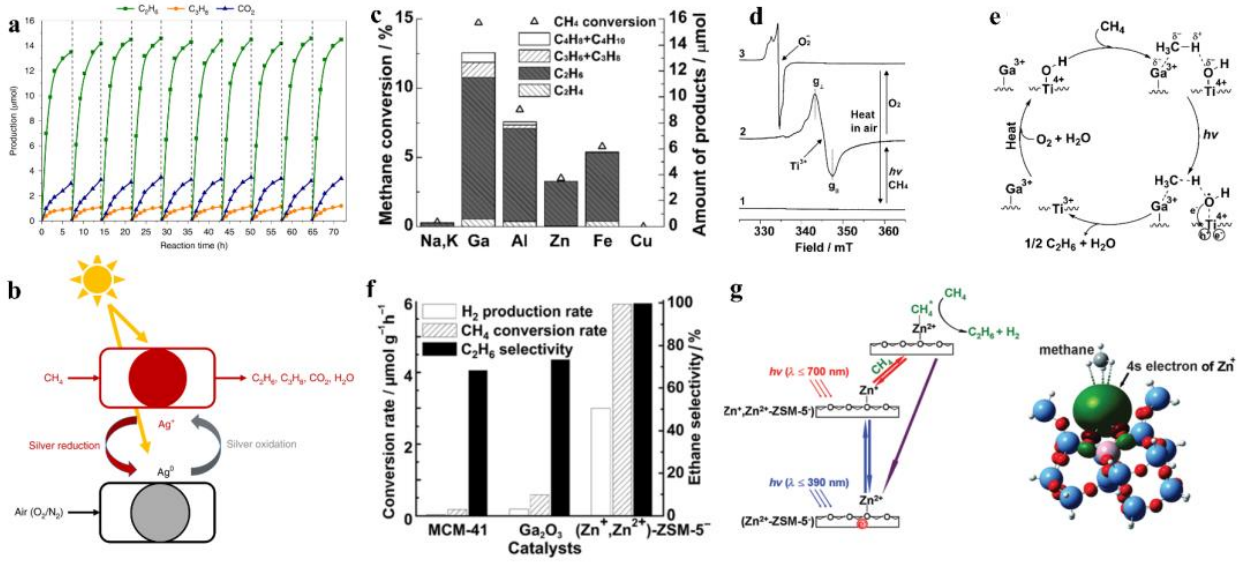


Figure 4. (**a**,**b**) Production and mechanism of Ag–HPW/TiO_2 catalyst in photocatalytic NOCM [2], copyright 2020, Springer Nature. (**c**,**d**) CH_4 conversion and product distribution were obtained in the photo-driven CH_4 activation reaction over various substrates under direct irradiation. From left to right: Na, K-ETS-10-0.2, Ga-ETS-10-0.2, Al-ETS-10-0.2, Zn-ETS-10-0.2, Fe-ETS-10-0.2, and Cu-ETS-10-0.2 [41], (**e**) EPR results of Ga-ETS-10-0.2 [41], copyright 2012, John Wiley and Sons. (**f**) CH_4 conversion and C_2H_6 selectivity of Zn^{2+}-ZSM-5^- catalyst [44], and (**g**) mechanism of Zn^{2+}-ZSM-5^- catalyst in photocatalytic NOCM [44]. Copyright 2011, John Wiley and Sons.

Li et al. [41] replaced Ga cations on the titanate framework (ETS-10, one-dimensional TiO_2 nanowires surrounding SiO_2) to obtain C_2H_6 selectivity of up to 70%. The study showed that CH_4 is adsorbed on the Ga site and the holes are captured by the -OH group. Then, hydroxyl radical (•OH) forms by attacking the C-H bond to generate $\bullet CH_3$. Subsequently, the same kind of groups of $\bullet CH_3$ are coupled to form C_2H_6(Figure 4d). At the same time, Ti^{4+} captures electrons to form Ti^{3+}, and Ti^{3+} further transfers its electrons to the lattice oxygen to form the interaction between superoxide radicals (O^{2-}) and H_2O (Figure 4c,d). Later, Li et al. [44] designed an electron delocalization state in the Zn^{2+}-ZSM-5^- catalyst, achieving a selectivity of C_2H_6 close to 100%. UV light-excited free electrons transform to the 4s orbital of Zn^{2+} to form Zn^+. Zn^+ attracts the H atom of the CH_4 molecule, then the anti-bond orbital obtains the 4s orbital electrons of Zn^+. This facilitates the desorption of a large number of protons and induces C-C coupling to form C_2H_6 (Figure 4f–g).

Ga_2O_3 with a wide band gap can withstand a strong electric field to polarize CH_4 molecules, and its cluster center bridges oxygen center radicals to promote the decomposition of CH_4 molecules under mild conditions [52]. In 2008, Yuliati et al. [45] achieved a selectivity of 94% for C_2H_6 on $Ga_{(0.1)}/SiO_2$ catalyst. The tetrahedral coordinated Ga_2O_3 active site selectively activated CH_4 molecules by limiting electrons in the Si-O bond through the Si-O-Ga structure. This is distinct from the electron transfer from O^{2-} to Ga^{3+} during photoexcitation, which is more conducive to the selective generation of C_2H_6. Moreover, Pratap Singh et al. [32] found in 2020 that increasing light intensity can not only promote the activation of the C-H bond but also accelerate the photooxidation reaction of $\bullet CH_3$ ($\bullet CH_3 + 3h^+ \rightarrow C + 3H^+$)(Figure 5a), which is not beneficial for forming C_2H_6.

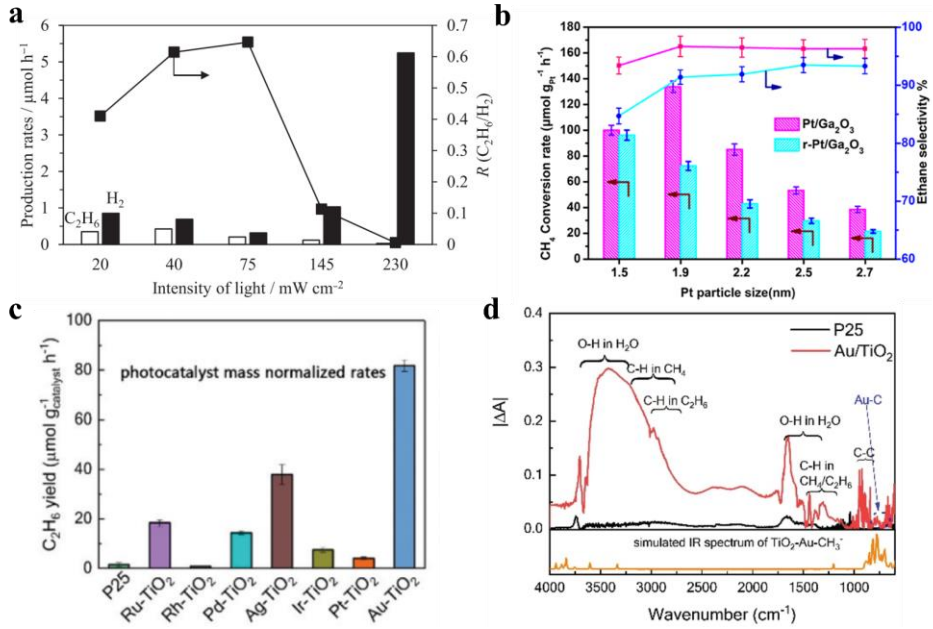


Figure 5. (**a**) Production rates on Pd/Ga_2O_3 with different light intensities [32], copyright 2011, Elsevier. (**b**) Photocatalytic reaction conversion and selectivity of Pt/Ga_2O_3 [46], copyright 2021, American Chemical Society. (**c**) C_2H_6 yield over TiO_2 catalysts supported by different noble metals in NOCM [53], and (**d**) IR spectra over Au/TiO_2 and P25 [53]. Copyright 2020, Royal Society of Chemistry.

Zhang et al. [46] studied the influence of the size effect of the active metal Pt. The catalytic activity showed a volcanic trend when the crystal size of Pt increased from 1.5 nm to 2.7 nm, and the maximum selectivity of C_2H_6 reached 90%. Small grain size is favorable for $Pt^{\delta+}$ transfer of photogenerated holes from Ga_2O_3 to adsorbed CH_4 molecules. Though the selectivity of C_2H_6 on metal-modified Ga_2O_3 is not low, its CH_4 conversion is not high (Figure 5b). Wu et al. [48] reported that Ga doping increased the free electron concentration on the Pt site. More Pt^0 can effectively dissociate the C-H bond. Furthermore, the Mott–Schottky heterojunction formed at Pt-TiO_2 accelerates the separation of the photogenerated carrier. Thus, the selectivity of C_2H_6 is 90% and the conversion of CH_4 is 28% on the *n*-type semiconductor Pt/HGTS catalyst (HGTS: Ga doped TiO_2-SiO_2). Lang et al. [53] found that the lower the interface potential of metal modification, the more difficult the recombination of photogenerated carriers, which is more conducive to enhancing catalytic performance. By comparing a series of TiO_2 (P25) catalysts modified by precious metals (Ru, Rh, Pd, Ag, Ir, Pt, and Au), it was found that the interface potential on Au-TiO_2 is the lowest, which is more conducive to rapid electron migration to activate CH_4 molecules. Consequently, the yield of C_2H_6 can reach 81.7 μmol g^{-1} h^{-1} on the Au-TiO_2 catalyst (Figure 5c,d).

Generally, photogenerated holes used to activate CH_4 are mainly concentrated at the lattice oxygen sites of metal oxide semiconductors, which makes CH_4 prone to overoxidation by lattice oxygen atoms to produce CO, CO_2, and other by-products. Xiong et al. [54] proposed the single-atom coordination method to regulate the valence band electronic structure of the Pd/TiO_2 catalyst. This resulted in a selectivity of up to 94.3% for C_2H_6, a C_2H_6 yield of 0.91 mmol g^{-1} h^{-1}, and H_2 products with an equal stoichiometric ratio (Figure 6). Photogenerated holes were clustered on the "Pd-O_4" coordination structure, thus reducing the contribution of the oxygen site to the valence band and improving the stability of lattice oxygen. This was shown to improve photocatalytic performance and reduce excessive oxidation in NOCM.

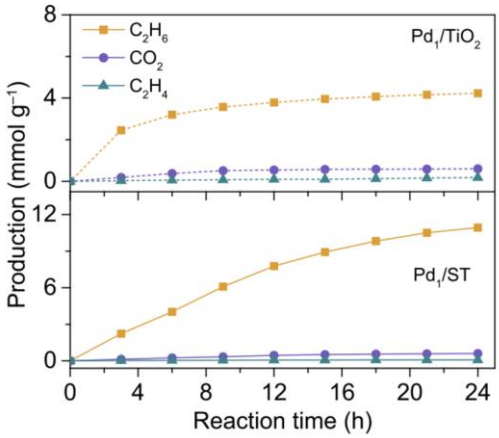


Figure 6. The comparison of production rate between Pd_1/TiO_2 and Pd_1/ST [54]. Copyright 2022, Springer Nature.

In addition, some other studies have found that an increase in CH_4 pressure in the reaction system (from 0.27 kPa to 0.49 KPa) can reduce the catalytic activity [36]. Furthermore, the type of light source, light intensity, the reaction device, temperature, and pressure of the reaction system are all important factors affecting the anaerobic coupling of photocatalytic CH_4.

4. Conclusions and Outlook

Direct conversion of CH_4 to C_2H_6 and H_2 has gained much attention due to its low cost, low carbonization, and other benefits. This review seeks to systematically analyze the development of thermal and photocatalytic NOCM, including the study of material properties and the exploration of reaction mechanisms. In contrast to other CH_4 conversions, non-oxidative coupling of CH_4 generates many by-products.

In traditional thermal catalytic NOCM, the C-H bond of CH_4 is broken through the application of high-temperature thermal energy. The range of 1053–1123 K is more conducive to the selective generation of C_2H_6, since it is an optimal balance between breaking the C-H bond and the CH_3-CH_3 coupling progress. However, with increasing temperature, the adsorption of methyl (-CH_3) on the precious metal catalysts surface weakens and the formation of intermediates such as -CH_2, -C_2H_3, and -C_2H_2 accelerates, thereby reducing the selectivity of C_2H_6. Non-precious metal catalysts, on the other hand, can promote the C-C coupling of CH_4 through the "restriction strategy" or "metal price change strategy" to obtain the target products of C_2H_6 and H_2.

Photochemical reactions driving NOCM can break the restriction of thermodynamic equilibrium at mild temperatures. Metal-oxide-based catalysts which do not have the inherent characteristics of semiconductors can be applied for photocatalytic NOCM, whereby CH_4 is directly converted from the ground state to the excited state under solar energy, thereby promoting the formation of adsorbed protons (H) and adsorbed •CH_3. This is achieved by dispersing highly active centers on non-photoresponsive insulator supports and localizing them on specific sites through the interaction between active components and supports. Additionally, it is useful for metal-modified catalysts to broaden the light response region and improve the conversion efficiency of solar energy. This can generate hot electrons or local electric fields to activate the C-H bond of CH_4. The metal, as an electron donor, undergoes the change from Me^{1+x} to Me^{x} during the reaction. Furthermore, hydroxyl radical (•OH) can be generated to attack the C-H bond to generate •CH_3 on metal-modified catalysts.

There are many by-products in the NOCM process, and the conversion efficiency of CH_4 is still relatively low. Thus, further research is warranted. In view of this, we propose the following methods for creating a photocatalyst for the NOCM reaction: (1) Developing in-situ technologies, such as X-ray Absorption Fine Structure (XAFS), X-ray Photoelectron

Spectroscopy (XPS), and Diffuse Reflectance Fourier Transform Infrared Spectroscopy (DRIFTS), to investigate the structural changes of intermediates and catalysts in an ultra-short time scale, which could help to distinguish between thermal and photocatalytic effects. (2) The laboratory typically utilizes Xe lamps as the solar energy source, limiting the use of sunlight of different wavebands. To improve the efficiency of solar energy conversion and utilization, researchers could consider using solar simulators for indoor testing, or solar concentrators to directly convert and utilize solar energy. (3) More research should focus on bimetallic catalysts to improve C_2H_6 selectivity by exploiting the synergistic effects of different metals. It is important to further elucidate the reaction mechanism of cocatalysts.

Author Contributions: J.W. and Z.R. contributed equally. Editing and review, J.W. and Z.R.; Review, Y.C.; Supervision, F.W., Z.H. and Y.Z. All authors have read and agreed to the published version of the manuscript.

Funding: This work has been financially supported by the National Natural Science Foundation of China (No. 202209136), the Sichuan Provincial International Cooperation Project (No. 22ZDYF3690, 2021YFH0055 and 2022YFH0084), the Cheung Kong Scholars Program of China, the Science Project of SWPU (No. 2021JBGS10), Central Government Funds of Guiding Local Scientific and Technological Development for Sichuan Province (No. 2021ZYD0035).

Data Availability Statement: Data sharing is not applicable to this article. No new data were created or analyzed in this study.

Conflicts of Interest: The authors declare no conflict of interest.

References

1. Kerr, R.A. Natural Gas From Shale Bursts Onto the Scene. *Science* **2010**, *328*, 1624–1626. [CrossRef] [PubMed]
2. Yu, X.; Zholobenko, V.L.; Moldovan, S.; Hu, D.; Wu, D.; Ordomsky, V.V.; Khodakov, A.Y. Stoichiometric methane conversion to ethane using photochemical looping at ambient temperature. *Nat. Energy* **2020**, *5*, 511–519. [CrossRef]
3. Montzka, S.A.; Dlugokencky, E.J.; Butler, J.H. Non-CO_2 greenhouse gases and climate change. *Nature* **2011**, *476*, 43–50. [CrossRef] [PubMed]
4. Yang, M.; Li, S.; Chen, G. High-temperature steam reforming of methanol over ZnO–Al_2O_3 catalysts. *Appl. Catal. B* **2011**, *101*, 409–416. [CrossRef]
5. Hosseini, S.E.; Wahid, M.A. Hydrogen production from renewable and sustainable energy resources: Promising green energy carrier for clean development. *Renew. Sustain. Energy Rev.* **2016**, *57*, 850–866. [CrossRef]
6. Najari, S.; Saeidi, S.; Concepcion, P.; Dionysiou, D.D.; Bhargava, S.K.; Lee, A.F.; Wilson, K. Oxidative dehydrogenation of ethane: Catalytic and mechanistic aspects and future trends. *Chem. Soc. Rev.* **2021**, *50*, 4564–4605. [CrossRef]
7. Xiao, Y.; Varma, A. Highly Selective Nonoxidative Coupling of Methane over Pt-Bi Bimetallic Catalysts. *ACS Catal.* **2018**, *8*, 2735–2740. [CrossRef]
8. Julian, I.; Ramirez, H.; Hueso, J.L.; Mallada, R.; Santamaria, J. Non-oxidative methane conversion in microwave-assisted structured reactors. *Chem. Eng. J.* **2019**, *377*, 119764. [CrossRef]
9. Wang, G.; Mu, X.; Li, J.; Zhan, Q.; Qian, Y.; Mu, X.; Li, L. Light-induced Nonoxidative Coupling of Methane using Stable Solid-Solutions. *Angew. Chem. Int. Ed. Engl.* **2021**, *13*, 20760–20764. [CrossRef]
10. Meng, L.; Chen, Z.; Ma, Z.; He, S.; Hou, Y.; Li, H.-H.; Yuan, R.; Huang, X.-H.; Wang, X.; Wang, X.; et al. Gold plasmon-induced photocatalytic dehydrogenative coupling of methane to ethane on polar oxide surfaces. *Energy Environ. Sci.* **2018**, *11*, 294–298. [CrossRef]
11. Huang, K.; Miller, J.B.; Huber, G.W.; Dumesic, J.A.; Maravelias, C.T. A General Framework for the Evaluation of Direct Nonoxidative Methane Conversion Strategies. *Joule* **2018**, *2*, 349–365. [CrossRef]
12. Bajec, D.; Kostyniuk, A.; Pohar, A.; Likozar, B. Nonoxidative methane activation, coupling, and conversion to ethane, ethylene, and hydrogen over Fe/HZSM-5, Mo/HZSM-5, and Fe–Mo/HZSM-5 catalysts in packed bed reactor. *Int. J. Energy Res.* **2019**, *43*, 6852–6868. [CrossRef]
13. Schwach, P.; Pan, X.L.; Bao, X.H. Direct Conversion of Methane to Value-Added Chemicals over Heterogeneous Catalysts: Challenges and Prospects. *Chem. Rev.* **2017**, *117*, 8497–8520. [CrossRef] [PubMed]
14. Amos, R.D. An accurateab initiostudy of the multipole moments and polarizabilities of methane. *Mol. Phys.* **1979**, *38*, 33–45. [CrossRef]
15. Reddy, P.V.L.; Kim, K.-H.; Song, H. Emerging green chemical technologies for the conversion of CH4 to value added products. *Renew. Sustain. Energy Rev.* **2013**, *24*, 578–585. [CrossRef]
16. Belgued, M.; Pareja, P.; Amariglio, A.; Amariglio, H. Conversion of Methane into Higher Hydrocarbons on Platinum. *Nature* **1991**, *352*, 789–790. [CrossRef]

17. Bajec, D.; Kostyniuk, A.; Pohar, A.; Likozar, B. Micro-kinetics of non-oxidative methane coupling to ethylene over Pt/CeO_2 catalyst. *Chem. Eng. J.* **2020**, *396*, 125182. [CrossRef]
18. Moya, S.F.; Martins, R.L.; Ota, A.; Kunkes, E.L.; Behrens, M.; Schmal, M. Nanostructured supported palladium catalysts—Non-oxidative methane coupling. *Appl. Catal. A* **2012**, *411–412*, 105–113. [CrossRef]
19. Li, Z.; Xiao, Y.; Chowdhury, P.R.; Wu, Z.; Ma, T.; Chen, J.Z.; Wan, G.; Kim, T.-H.; Jing, D.; He, P.; et al. Direct methane activation by atomically thin platinum nanolayers on two-dimensional metal carbides. *Nat. Catal.* **2021**, *4*, 882–891. [CrossRef]
20. Guo, X.; Fang, G.; Li, G.; Ma, H.; Fan, H.; Yu, L.; Ma, C.; Wu, X.; Deng, D.; Wei, M.; et al. Direct, Nonoxidative Conversion of Methane to Ethylene, Aromatics, and Hydrogen. *Science* **2014**, *344*, 616–619. [CrossRef]
21. Xie, P.; Pu, T.; Nie, A.; Hwang, S.; Purdy, S.C.; Yu, W.; Su, D.; Miller, J.T.; Wang, C. Nanoceria-Supported Single-Atom Platinum Catalysts for Direct Methane Conversion. *ACS Catal.* **2018**, *8*, 4044–4048. [CrossRef]
22. Kim, S.K.; Kim, H.W.; Han, S.J.; Lee, S.W.; Shin, J.; Kim, Y.T. Mechanistic and microkinetic study of non-oxidative methane coupling on a single-atom iron catalyst. *Commun. Chem.* **2020**, *3*, 58. [CrossRef] [PubMed]
23. Dipu, A.L.; Ohbuchi, S.; Nishikawa, Y.; Iguchi, S.; Ogihara, H.; Yamanaka, I. Direct Nonoxidative Conversion of Methane to Higher Hydrocarbons over Silica-Supported Nickel Phosphide Catalyst. *ACS Catal.* **2019**, *10*, 375–379. [CrossRef]
24. Han, S.J.; Lee, S.W.; Kim, H.W.; Kim, S.K.; Kim, Y.T. Nonoxidative Direct Conversion of Methane on Silica-Based Iron Catalysts: Effect of Catalytic Surface. *ACS Catal.* **2019**, *9*, 7984–7997. [CrossRef]
25. Soulivong, D.; Norsic, S.; Taoufik, M.; Cope'ret, C.; Thivolle-Cazat, J.; Chakka, S.; Basset, J.-M. Non-Oxidative Coupling Reaction of Methane to Ethane and Hydrogen Catalyzed by the Silica-Supported Tantalum Hydride: $(tSiO)_2Ta$-H. *J. Am. Chem. Soc.* **2008**, *130*, 5044–5045. [CrossRef]
26. Moya, S.F.; Martins, R.L.; Schmal, M. Monodispersed and nanostructrured Ni/SiO_2 catalyst and its activity for non oxidative methane activation. *Appl. Catal. A* **2011**, *396*, 159–169. [CrossRef]
27. Zhang, X.; Deng, J.; Pupucevski, M.; Impeng, S.; Yang, B.; Chen, G.; Kuboon, S.; Zhong, Q.; Faungnawakij, K.; Zheng, L.; et al. High-Performance Binary Mo–Ni Catalysts for Efficient Carbon Removal during Carbon Dioxide Reforming of Methane. *ACS Catal.* **2021**, *11*, 12087–12095. [CrossRef]
28. Liu, Y.; Liu, J.C.; Li, T.H.; Duan, Z.H.; Zhang, T.Y.; Yan, M.; Li, W.L.; Xiao, H.; Wang, Y.G.; Chang, C.R.; et al. Unravelling the Enigma of Nonoxidative Conversion of Methane on Iron Single-Atom Catalysts. *Angew. Chem. Int. Ed. Engl.* **2020**, *59*, 18586–18590. [CrossRef]
29. Kashaboina, U.; Nishikawa, Y.; Wakisaka, Y.; Sirisit, N.; Nagamatsu, S.-I.; Bao, D.; Ariga-Miwa, H.; Takakusagi, S.; Inami, Y.; Kuriyama, F.; et al. Metamorphosis-like Transformation during Activation of In/SiO2 Catalyst for Non-oxidative Coupling of Methane: In Situ X-ray Absorption Fine Structure Analysis. *Chem. Lett.* **2019**, *48*, 1145–1147. [CrossRef]
30. Al Rashid, M.H.; Dipu, A.; Nishikawa, Y.; Ogihara, H.; Inami, Y.; Obuchi, S.; Yamanaka, I.; Nagamatsu, S.; Kido, D.; Asakura, K. Active Phase Structure of the SiO_2-supported Nickel Phosphide Catalysts for Non-oxidative Coupling of Methane (NOCM) Reactions. *E-J. Surf. Sci. Nanotechnol.* **2020**, *18*, 24–27. [CrossRef]
31. Lin, X.; Xi, Y.; Zhang, G.; Phillips, D.L.; Guo, W. A Reaction Mechanism of Methane Coupling on a Silica-Supported Single-Site Tantalum Catalyst. *Organometallics* **2014**, *33*, 2172–2181. [CrossRef]
32. Singh, S.P.; Anzai, A.; Kawaharasaki, S.; Yamamoto, A.; Yoshida, H. Non-oxidative coupling of methane over Pd-loaded gallium oxide photocatalysts in a flow reactor. *Catal. Today* **2020**, *375*, 264–272. [CrossRef]
33. Baltrusaitis, J.; Jansen, I.; Schuttlefield Christus, J.D. Renewable energy based catalytic CH4 conversion to fuels. *Catal. Sci. Technol.* **2014**, *4*, 2397–2411. [CrossRef]
34. Kato, Y.; Yoshida, H.; Hattorib, T. Photoinduced non-oxidative coupling of methane over silica-alumina and alumina around room temperature. *Chem. Commun.* **1998**, *21*, 2389–2390. [CrossRef]
35. Yuliati, L.; Tsubota, M.; Satsuma, A.; Itoh, H.; Yoshida, H. Photoactive sites on pure silica materials for nonoxidative direct methane coupling. *J. Catal.* **2006**, *238*, 214–220. [CrossRef]
36. Yoshida, H.; Chaskar, M.G.; Kato, Y.; Hattori, T. Active sites on silica-supported zirconium oxide for photoinduced direct methane conversion and photoluminescence. *J. Photochem. Photobiol. A* **2003**, *160*, 47–53. [CrossRef]
37. Kato, Y.; Matsushita, N.; Yoshida, H.; Hattori, T. Highly active silica–alumina–titania catalyst for photoinduced non-oxidative methane coupling. *Catal. Commun.* **2002**, *3*, 99–103. [CrossRef]
38. Yoshida, H.; Matsushita, N.; Kato, Y.; Hattori, T. Synergistic Active Sites on SiO_2-Al_2O_3-TiO_2 Photocatalysts for Direct Methane Coupling. *J. Phys. Chem. B* **2003**, *107*, 8355–8362. [CrossRef]
39. Chen, Z.; Wu, S.; Ma, J.; Mine, S.; Toyao, T.; Matsuoka, M.; Wang, L.; Zhang, J. Non-oxidative Coupling of Methane: N-type Doping of Niobium Single Atoms in $TiO_{(2)}$-$SiO_{(2)}$ Induces Electron Localization. *Angew. Chem. Int. Ed. Engl.* **2021**, *60*, 11901–11909. [CrossRef]
40. Yoshida, H.; Hamajima, T.; Kato, Y.; Shibata, J.; Satsuma, A.; Hattori, T. Active Ag species in MFI zeolite for direct methane conversion in the light and dark. *Res. Chem. Intermed.* **2003**, *29*, 7–9. [CrossRef]
41. Li, L.; Cai, Y.Y.; Li, G.D.; Mu, X.Y.; Wang, K.X.; Chen, J.S. Synergistic effect on the photoactivation of the methane C-H bond over Ga(3+)-modified ETS-10. *Angew. Chem. Int. Ed. Engl.* **2012**, *51*, 4702–4706. [CrossRef] [PubMed]
42. Yuliati, L.; Hamajima, T.; Hattori, T.; Yoshida, H. Highly dispersed Ce(III) species on silica and alumina as new photocatalysts for non-oxidative direct methane coupling. *Chem. Commun. (Camb)* **2005**, *38*, 4824–4826. [CrossRef] [PubMed]

43. Yuliati, L.; Hamajima, T.; Hattori, T.; Yoshida, H. Nonoxidative Coupling of Methane over Supported Ceria Photocatalysts. *J. Phys. Chem. C* **2008**, *112*, 7223–7232. [CrossRef]
44. Li, L.; Li, G.D.; Yan, C.; Mu, X.Y.; Pan, X.L.; Zou, X.X.; Wang, K.X.; Chen, J.S. Efficient sunlight-driven dehydrogenative coupling of methane to ethane over a Zn(+)-modified zeolite. *Angew. Chem. Int. Ed. Engl.* **2011**, *50*, 8299–8303. [CrossRef]
45. Yuliati, L.; Hattori, T.; Itoh, H.; Yoshida, H. Photocatalytic nonoxidative coupling of methane on gallium oxide and silica-supported gallium oxide. *J. Catal.* **2008**, *257*, 396–402. [CrossRef]
46. Ma, J.; Tan, X.; Zhang, Q.; Wang, Y.; Zhang, J.; Wang, L. Exploring the Size Effect of Pt Nanoparticles on the Photocatalytic Nonoxidative Coupling of Methane. *ACS Catal.* **2021**, *11*, 3352–3360. [CrossRef]
47. Singh, S.P.; Yamamoto, A.; Fudo, E.; Tanaka, A.; Kominami, H.; Yoshida, H. A Pd-Bi Dual-Cocatalyst-Loaded Gallium Oxide Photocatalyst for Selective and Stable Nonoxidative Coupling of Methane. *ACS Catal.* **2021**, *11*, 13768–13781. [CrossRef]
48. Wu, S.; Tan, X.; Lei, J.; Chen, H.; Wang, L.; Zhang, J. Ga-Doped and Pt-Loaded Porous TiO_2-SiO_2 for Photocatalytic Nonoxidative Coupling of Methane. *J. Am. Chem. Soc.* **2019**, *141*, 6592–6600. [CrossRef]
49. Yoshida, H.; Matsushita, N.; Kato, Y.; Hattori, T. Active sites in sol–gel prepared silica-alumina for photoinduced non-oxidative methane coupling. *Phys. Chem. Chem. Phys.* **2002**, *4*, 2459–2465. [CrossRef]
50. Talebi, P.; Kistanov, A.A.; Rani, E.; Singh, H.; Pankratov, V.; Pankratova, V.; King, G.; Huttula, M.; Cao, W. Unveiling the role of carbonate in nickel-based plasmonic core@shell hybrid nanostructure for photocatalytic water splitting. *Appl. Energy* **2022**, *322*, 119461. [CrossRef]
51. Song, H.; Meng, X.; Wang, Z.-J.; Liu, H.; Ye, J. Solar-Energy-Mediated Methane Conversion. *Joule* **2019**, *3*, 1606–1636. [CrossRef]
52. Schwarz, H.; Shaik, S.; Li, J. Electronic Effects on Room-Temperature, Gas-Phase C-H Bond Activations by Cluster Oxides and Metal Carbides: The Methane Challenge. *J. Am. Chem. Soc.* **2017**, *139*, 17201–17212. [CrossRef] [PubMed]
53. Lang, J.; Ma, Y.; Wu, X.; Jiang, Y.; Hu, Y.H. Highly efficient light-driven methane coupling under ambient conditions based on an integrated design of a photocatalytic system. *Green Chem.* **2020**, *22*, 4669–4675. [CrossRef]
54. Zhang, W.; Fu, C.; Low, J.; Duan, D.; Ma, J.; Jiang, W.; Chen, Y.; Liu, H.; Qi, Z.; Long, R.; et al. High-performance photocatalytic nonoxidative conversion of methane to ethane and hydrogen by heteroatoms-engineered TiO2. *Nat. Commun.* **2022**, *13*, 2806. [CrossRef]

Disclaimer/Publisher's Note: The statements, opinions and data contained in all publications are solely those of the individual author(s) and contributor(s) and not of MDPI and/or the editor(s). MDPI and/or the editor(s) disclaim responsibility for any injury to people or property resulting from any ideas, methods, instructions or products referred to in the content.